DOI: 10.22499/3.6901.015

JSHESS early online view

This article has been accepted for publication in the *Journal of Southern Hemisphere Earth Systems Science* and undergone full peer review. It has not been through the copy-editing, typesetting and pagination, which may lead to differences between this version and the final version.

Corresponding author: Shuan

g Wang, Bureau of Meteorology, Sydney

Email: S.Wang@bom.gov.au

Analysis of a Southerly Buster Event and Associated Solitary Waves

Shuang Wang[1, 2], Lance Leslie[1], Tapan Rai[1], Milton Speer[1] and Yuriy Kuleshov[3]

[1] University of Technology Sydney, Sydney, Australia
[2] Bureau of Meteorology, Sydney, Australia
[3] Bureau of Meteorology, Melbourne, Australia

(Manuscript submitted March 19, 2019)
Revised version submitted July 23, 2019

Corresponding author: Shuan

g Wang, Bureau of Meteorology, Sydney

Email: S.Wang@bom.gov.au

ABSTRACT

This paper is a detailed case study of the southerly buster of October 6-7, 2015, along the New South Wales coast. It takes advantage of recently available Himawari-8 high temporal- and spatial-resolution satellite data, and other observational data. The data analyses support the widespread view that the southerly buster is a density current, coastally trapped by the Great Dividing Range. In addition, it appears that solitary waves develop in this event because the prefrontal boundary layer is shallow and stable. A simplified density current model produced speeds matching well with observational southerly buster data, at both Nowra and Sydney airports. Extending the density current theory, to include inertia-gravity effects, suggests that the solitary waves travel at speeds approximately 20% faster than the density current. This speed difference is consistent with the high-resolution satellite data, which shows the solitary waves moving increasingly ahead of the leading edge of the density current.

Key words: Coastally Trapped Disturbance, Southerly Buster, Density Currents, Solitary Waves

1. Introduction

Southerly busters (SBs) occur during the spring and summer months in southeast Australia, to the east of the Great Dividing Range (Fig.1), along the coast of New South Wales (NSW) from about 38ºS to 30ºS. They are strong, sudden and squally southerly wind surges (e.g., Colquhoun et al., 1985; McInnes and McBride, 1993; Reid and Leslie, 1999). The depth of the surge is generally less than 1km. The SB passage is notable for the typical wind shift from north-westerly to southerly, and for the sudden temperature decreases of up to 20ºC within minutes (Gentilli, 1969). More precisely, SBs are defined as, “squally wind change that produce strong southerly winds near the coast with gusts to at least 15m/s soon after their passages and which are not associated with a major depression over the Tasman Sea at New South Wales latitudes" (Colquhoun et al., 1985). Strong SBs (SSBs) are defined as those with wind gusts of at least 21m/s, which is the issuance criterion for airport warnings of expected damaging winds. SBs are particularly intense examples of thermally and orographically influenced cold fronts. They occur because inversions ahead of the cold front prevent the vertical escape of energy, and Coriolis effects trap the energy against the Great Dividing Range (GDR) (Colquhoun et al., 1985; Gill, 1977).

SBs also have been investigated under other names. These designations include ducted coastal ridging, which is an atmospheric surge over coastal southeast Australia, moving at a speed of about 20m/s at the leading edge of the ridge (Holland and Leslie, 1986). The coastal ridging is initiated by a forced Kelvin-type edge wave which forms on the southwest end of the GDR, in coastal western Victoria, and is ducted, anticlockwise, around the coast. The ridge then is stabilized by inertial modification, and decays on a synoptic time scale of a few days (Holland and Leslie, 1986). Another widely used term is coastally trapped disturbances (CTDs), following the study by Gill (1977) of the coastal lows observed moving anticlockwise around southern Africa. Coastal lows are similar in structure to coastally trapped waves in the ocean. As in the case of SBs, inversion conditions typical of the area prevent the escape of energy upwards, and Coriolis effects trap energy against the high escarpment that borders the southern African coast. Hence, CTDs are produced

Figure 1: Topography of New South Wales Pacific Ocean coast from Nowra to Sydney, with the Great Dividing Range to the west of Nowra, Bellambi and Sydney in metres (m). The map includes the regional district boundaries and the elevation bands are in metres. The heights just west of Nowra (YNSW) typically are ~500m and west of Sydney Airport (YSSY) are ~1000m.

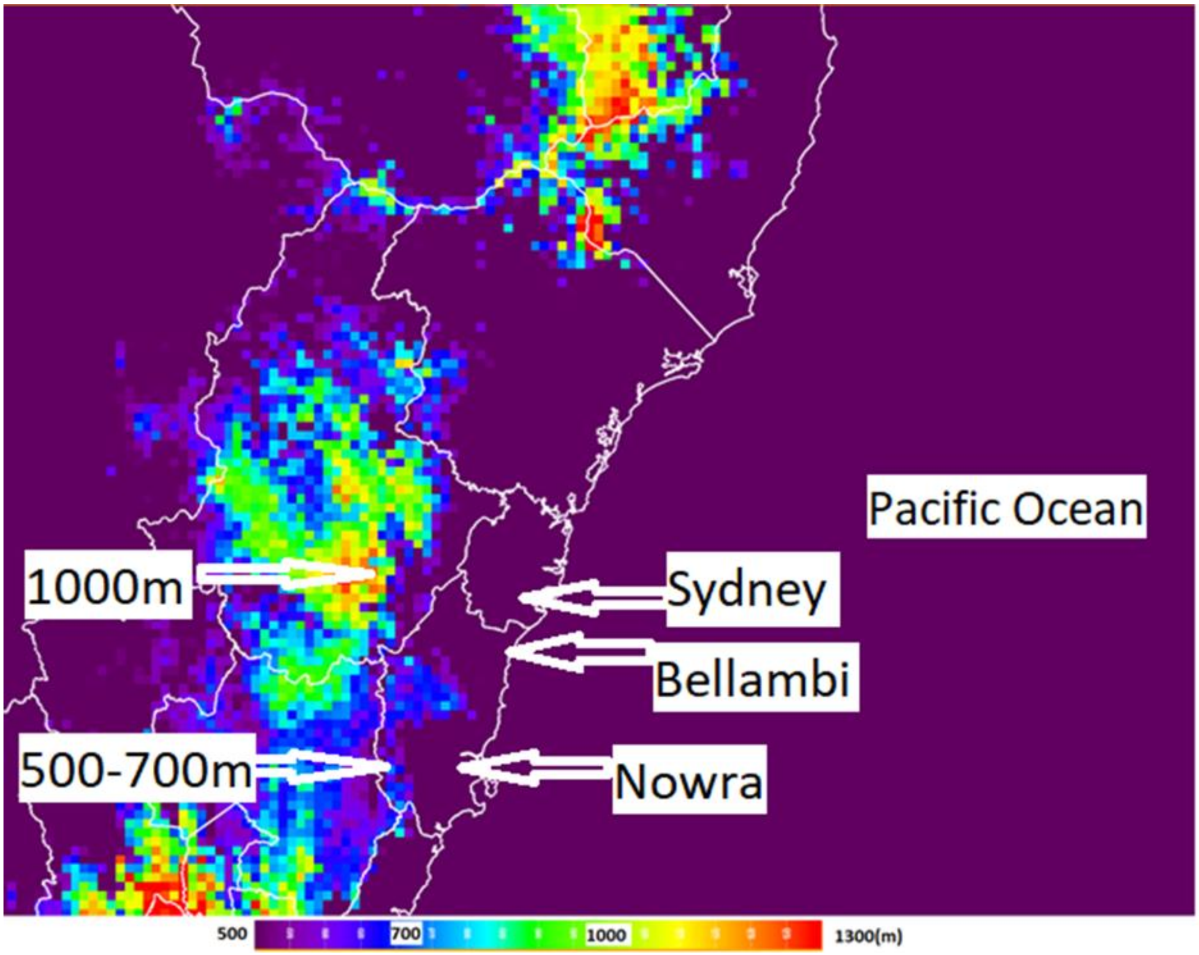

because low-level flow in the synoptic-scale systems cannot cross the escarpment (Gill, 1977). The term CTD also has been used frequently for south-eastern Australia SBs (e.g. Reason, 1994; Reason and Steyn, 1990; Reason and Steyn, 1992; Reason et al., 1999). Notably, the consensus is that the SB is a gravity current, also known as a density current, trapped against the coast by the Great Dividing Range (e.g., Baines, 1980, Mass and Albright, 1987; Egger and Hoinka, 1992; McInnes, 1993; Reid and Leslie, 1999). As such, it is initiated by a synoptic scale system and is generated by the density difference between the cooler southerly flow and the *in situ* warmer environment ahead of the surge.

Due to the rapid wind and temperature changes, SBs frequently are accompanied by low cloud, fog, thunderstorms and gusty winds. Consequently, SBs are a potential threat for human health, lives and property. In the case of aviation, there are numerous aircraft hazards that often result from the low-level wind shear associated with the SBs, especially during take-off or landing. The main consequences of wind shear include turbulence, violent air movement (e.g., abrupt up- and down-draughts, and swirling, or rotating, air patterns), sudden increases or reductions of airspeed, and rapid increases or decreases of groundspeed and/or drift. The strong winds and associated low level turbulence also are hazards for boating, especially as SBs occur along the populous southeast seaboard of Australia. For marine activities such as surfing, rock fishing and boating, each year marine rescue organizations respond to thousands of calls for assistance from NSW coastal waters; many are related to the passage of SBs, which can produce sudden strong to gale force coastal winds and generate dangerously high waves and choppy seas.

In this study, the SB event of October 6-7, 2015 is examined with the high temporal and spatial resolution observational data that was not available in the earlier studies mentioned above. As mentioned above, a SB is viewed as a density current advancing into a strongly stable *in situ* boundary layer which is comprised of warm summertime prefrontal continental air advection overlaying a cooler sea. Frequently a roll vortex is generated, which extends ahead of the cold front, in about half of observed SBs (Colquhoun, 1985; http://www.eumetrain.org). The head of the density current breaks away from the feeder flow supplying it with cold air and the pre-frontal boundary layer commonly is between 100m and 200m deep and, if the pre-frontal stable layer is deep and strong, the roll vortex can evolve as a solitary wave, or as a bore wave, that propagates on the stable layer.

2. Observations and Analysis

2.1 Station observations

On October 6, 2015, a southerly wind change (SC) propagated along the southeast coast of Australia. At Nowra Airport (YSNW), the winds were moderate (5-10m/s) west to north-westerly during the day, from 0000UTC (Coordinated Universal Time) to 0730UTC, due to the synoptic winds ahead of the trough. The winds became light and variable in the evening (0730UTC to 1200UTC), then trended to northwest drainage flow around or below 5 m/s before the SC occurred (Fig.2). At 1559UTC, the SC arrived at YSNW with southerly winds of 8m/s, gusting to 11m/s, at the automatic weather station (AWS) site which is 112km south of Sydney Airport (YSSY). At 1630UTC, the SC wind gusts touched 15m/s, thereby officially becoming a SB, then decreased over the following 90 minutes. The SC arrived at Sydney Airport (YSSY) at 1800UTC and became a SB just two minutes later. The wind gusts reached 21m/s which met the criterion for an airport warning at YSSY (Fig. 3) and Table 1. At YSSY, ahead of the SC, there was light to moderate northwest drainage flow around 3-4m/s; at 1800UTC, the observations showed nil significant cloud and the wind direction changed from northwest to south to southwest, the wind speeds picked up at 1802UTC with gusts to 15m/s, hence reaching SB levels. Approximately 16 minutes later, at 1816UTC, some low clouds developed at around 300m; at the same time, the visibility dropped to about 2300m, or 7000 feet (Fig. 4). Another key signature was a sudden pressure rise of up to 6hPa after the SC, within three hours, at both YSNW and YSSY. This pressure rise had become noticeably steeper, starting at Mt Gambier and reached a maximum amplitude and steepness from Nowra (6.2hPa) to YSSY (6.4hPa). The rapid pressure rises associated with the coastal ridging that occur behind the SC are a signature feature of the main CTD (Holland and Leslie, 1986).

Figure 2: Observations of wind change from 0000UTC to 2330UTC on October 6, 2015 at Nowra (YSNW). Time in UTC for horizontal axis, wind directions in degrees for primary vertical axis (left), wind speed gusts in m/s for secondary vertical axis (right). Wind speeds (orange clustered columns, m/s), Wind gusts (grey clustered columns, m/s), Wind directions (blue lines, degrees).

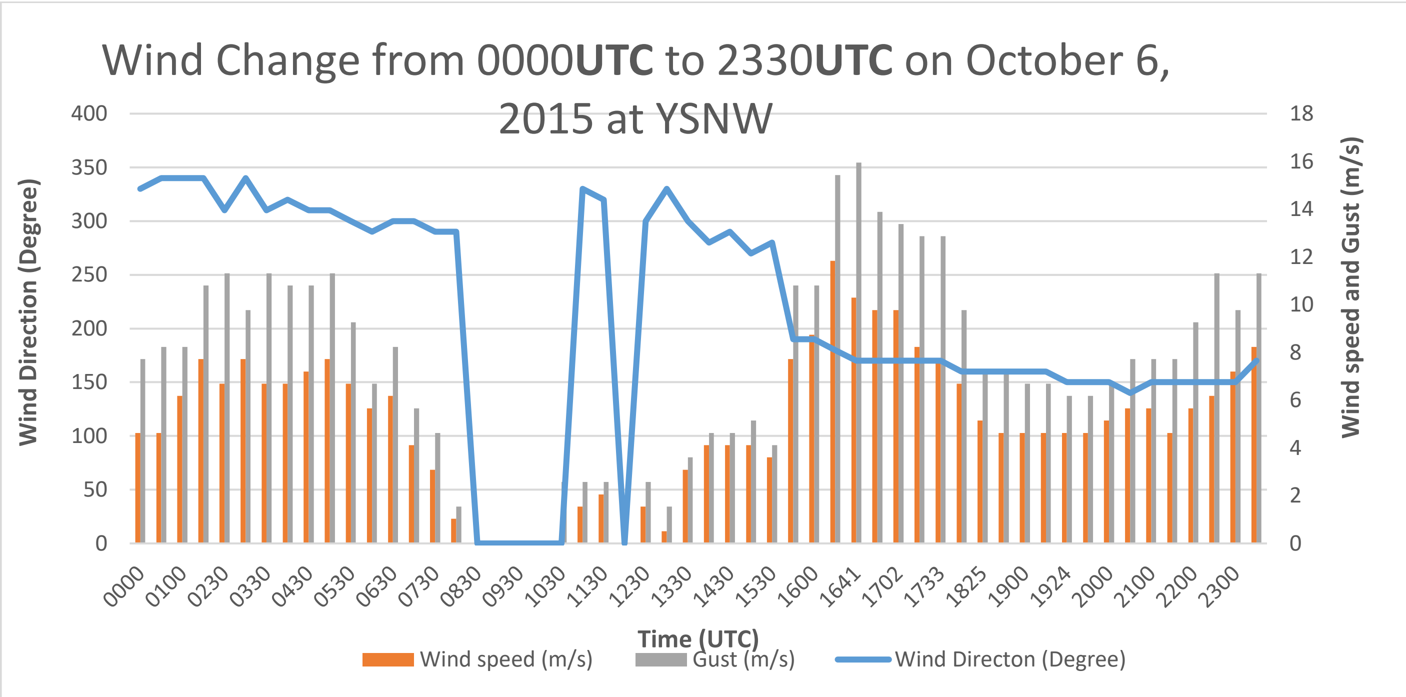

Figure 3: As in Figure 2, except at Sydney (YSSY) from 0900UTC to 2400UTC on October 6, 2015.

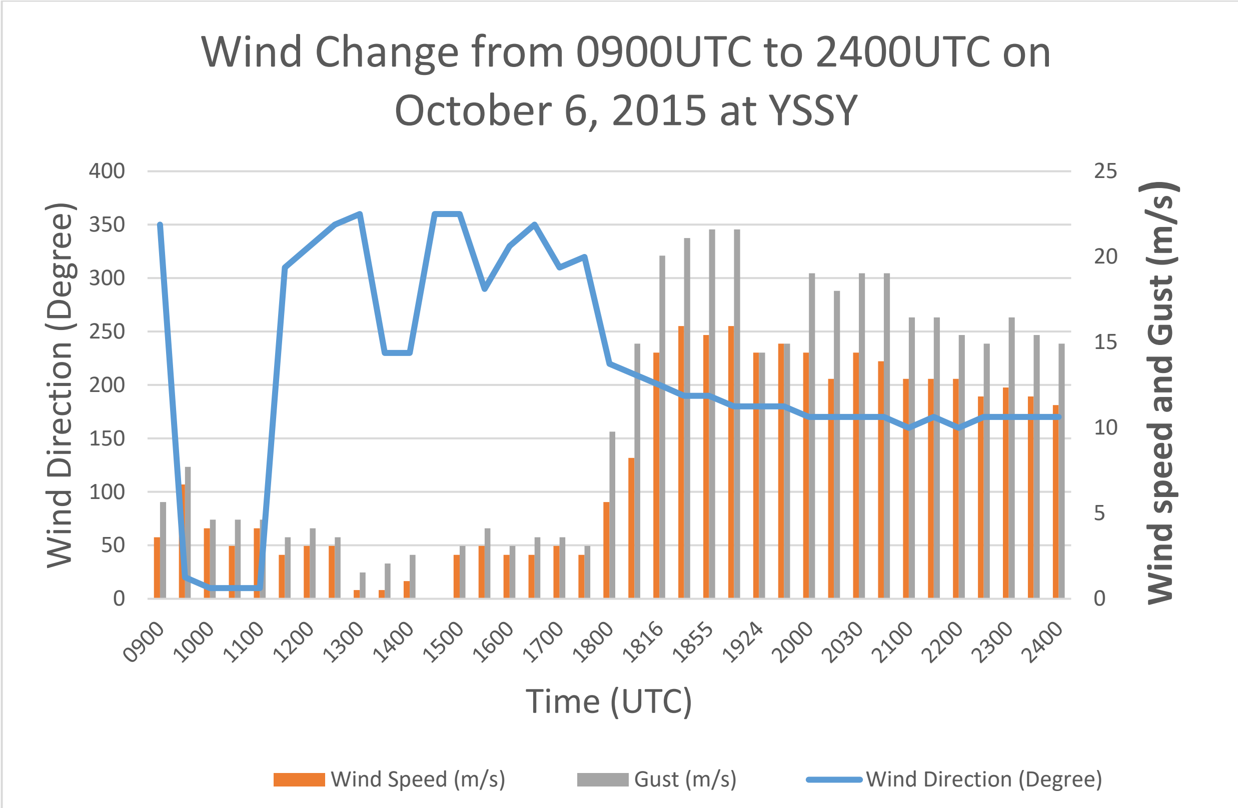

Figure 4: Observations of wind, visibility and cloud change from 0900UTC to 2400UTC on October 6, 2015 at YSSY. Time in UTC for horizontal axis, wind speeds and wind gust in m/s for primary vertical axis (left), visibility in metres and cloud base in feet for secondary axis (right). Wind speeds (blue clustered columns in m/s), Wind gusts (orange clustered columns in m/s), Visibility (grey lines in metres), Cloud base (yellow lines in feet).

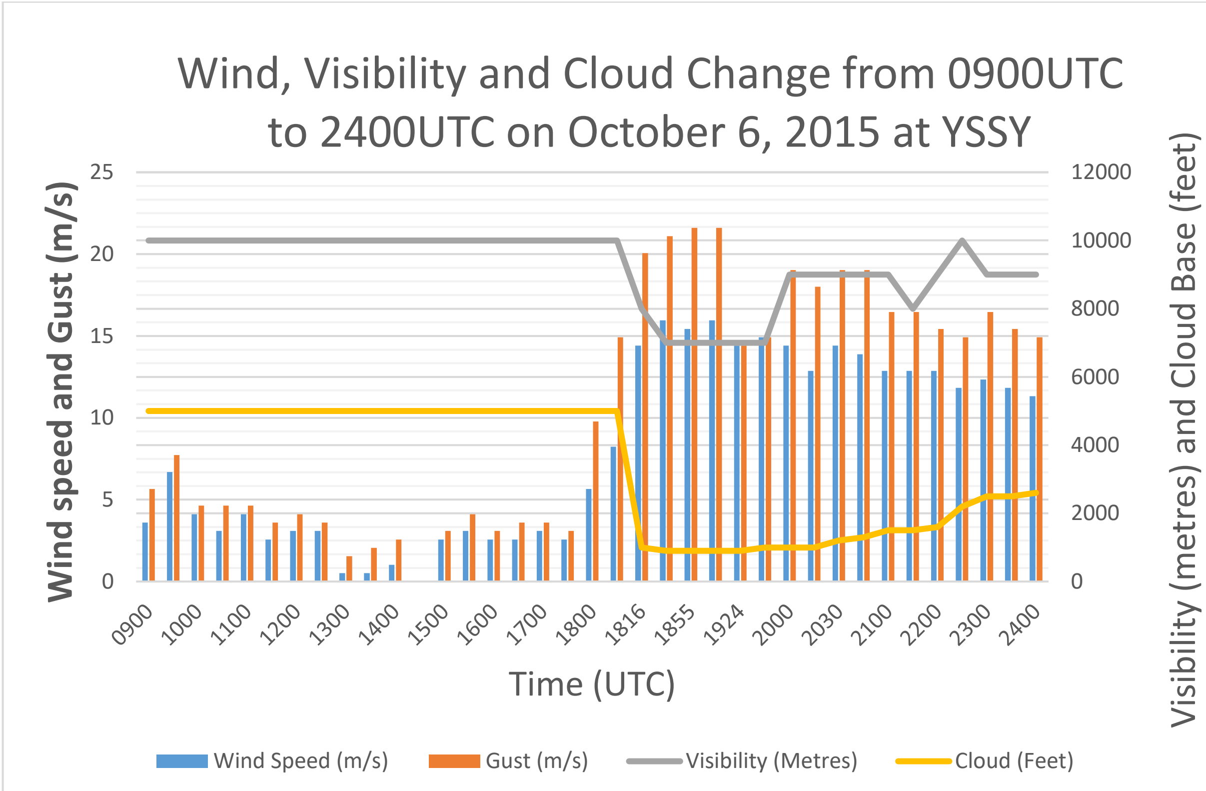

Table 1: Details of the wind changes at YSNW and YSSY. The southerly change (SC) and southerly buster (SB) time and maximum SB occurring time and winds details including wind direction (degrees), speed and gust (m/s): e.g., 19008G11 means the wind direction is 190 degrees, the mean wind speed is 08 m/s and the gust wind speed is 11m/s.

	SC time (UTC)	*SC winds (m/s)*	*SB time (UTC)*	*SB winds (m/s)*	*Maximum SB time (UTC)*	*Maximum SB winds (m/s)*
YSNW	1559	19008G11	1630	18012G17	1641	17010G16
YSSY	1800	22006G10	1802	21008G15	1900	18016G21

2.2 Synoptic Overview

The synoptic situation is obtained from archived upper-level and mean surface level pressure (MSLP) charts. At 850hPa on 0000UTC October 5, 2015, a high pressure system dominated much of southeast Australia with warm temperatures up to 19°C, while a low pressure system with cooler temperatures extended a NW-SE orientated trough from southwest of Australia, crossing the Southern Ocean south of Tasmania. At 1200UTC October 5, the high moved slowly southwest while the trough moved northeast. By 0000UTC October 6, the high pressure centre had moved over the Tasman Sea, and the trough was situated further to the northeast.

A phenomenon well-known to Australian meteorologists is the rapid establishment of a strong coastal ridge, which occurs when a Southern Ocean anticyclone approaches south-eastern Australia. This ridging is initiated by a high pressure surge which begins off the coast of southern Victoria, then moves rapidly along the NSW coast, and often travels along most the entire east coast of Australia, a distance of 2000-3000km. In contrast, the parent anticyclone moves only several hundred kilometres (Holland and Leslie, 1986). The MSLP charts from 0600UTC October 6 to 1800UTC October 7, 2015 are shown in Fig. 5. At 0600UTC October 6, coastal ridging was initiated at the south-western extremity of the GDR, between Mt Gambier and Cape Otway, associated with the northward movement of cold air behind a nearly zonal Southern Ocean front. East of Mt Gambier the cold flow was blocked by the southern slopes of the GDR, thereby driving the ducted disturbance eastwards along the Victorian coast. At 1200UTC October 6, the coastal ridging had propagated around the southeast corner of Australia and was located on the NSW coast, north of Gabo Island. At 1800UTC October 6, a strong high-pressure centre (1036hPa) was situated in the Great Australian Bight, with an inland trough west of the ranges and a frontal zone off eastern Australia, further extending the coastal ridge along the southeast NSW coast. At 0000UTC October

Figure 1: Synoptic weather charts from 0600UTC October 6 to 1800UTC October 7 on a) 0600 UTC October 6, 2015. b) 1200UTC October 6. 2015, c) 1800UTC October 6, 2015. d) 0000UTC October 7, 2015. e) 1200UTC October 7, 2015. f) 1800UTC October 7, 2015. Shown are contours of Mean Sea Level Pressure (MSLP) in intervals of 4hPa, local maxima and minima of MSLP, manually analysed cold fronts (solid lines with triangular barbs), and low pressure troughs (dashed lines). (Charts are from http://www.bom.gov.au/australia/charts/).

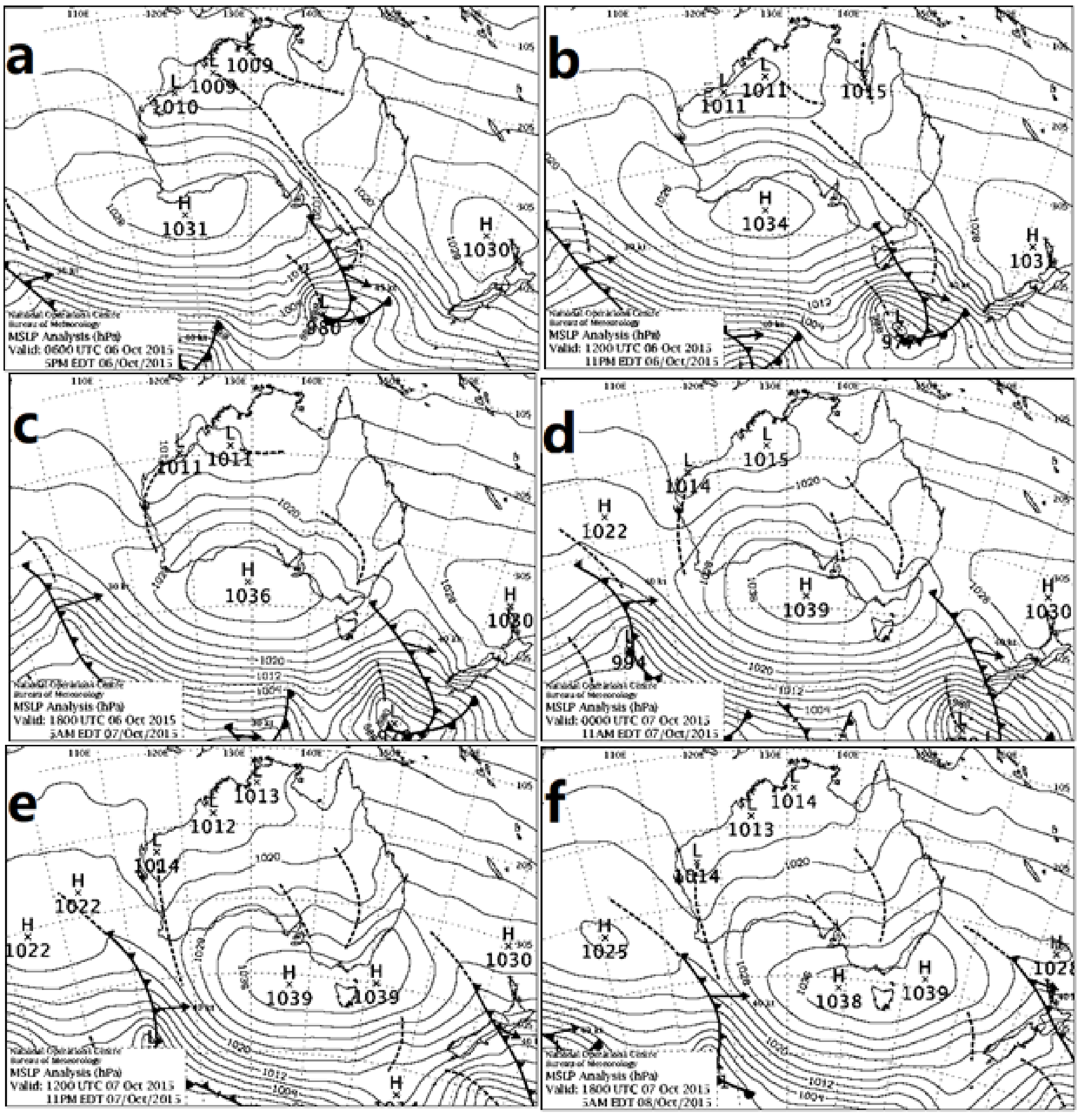

7, the cold front had continued moving northeast while the high pressure centre increased to 1039hPa, strengthening the ridge over southeast NSW. By 1200UTC and 1800UTC October 7, the original high pressure system had separated into two centres, with the parent high remaining over the Southern Ocean, and the second centre moving to the south of the Tasman Sea. The coastal ridging had extended along the entire NSW coast and entered southern Queensland.

2.3 Satellite Imagery

The Himawari-8 satellite image at 2140UTC on October 6 (Fig.6), reveals a possible roll cloud accompanying the SB offshore near Williamtown, extending to the southeast over the Tasman Sea. Ahead of the cold front cloud band, what appear to be shallow solitary waves are moving with the cold front cloud band. Clarke (1961) determined the mesoscale structure of the dry cold fronts using serial pilot balloon flights, radiosonde, and aircraft data. He found closed circulations (roll vortices) in the velocity field behind several fronts; in two cases, double circulations with the roll vortices were inferred (Clarke, 1961). A study of seventeen strong SBs over the period January 1972 to January 1978 was carried out by Colquhoun et al. (1985). Attempts were made to infer the structure of the 17 SBs from anemograph data and temperature profile measurements. The arrival of a clockwise rotating vortex (viewed from the west) was associated with an increase in wind

Figure 6: Himawari-8 satellite visible image at 2140UTC on October 6. 2015 over the New South Wales coast. Image is shown with the permission of the Australian Bureau of Meteorology. The AWS wind barbs show wind direction and speed in knots (red barbs), and the overlain boundaries of the Australian aviation regions (yellow lines). The green arrow indicates the leading edge of the SB, accompanied by a roll cloud. The yellow arrow points to the low cloud banking up against the escarpment of the range behind the passage of the SB over the eastern Great Dividing

Range. The pink arrow locates the parent cold front to the SB. The red arrow shows a possible train of solitary waves. The green circle shows a structure similar to the schematic representation in Fig. 7.

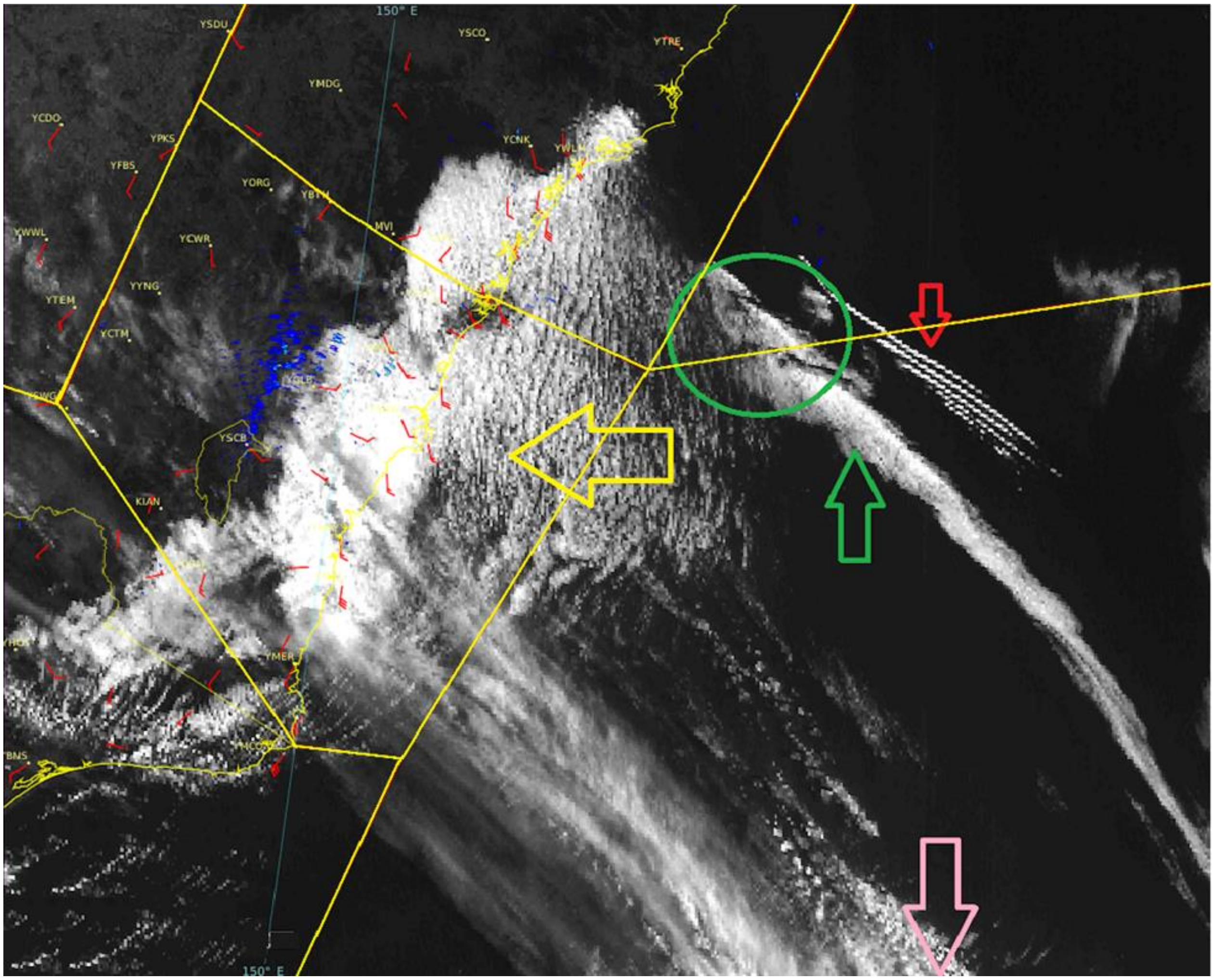

speed and instability and a decrease in temperature; the highest wind speed occurred under the circulation centre of the vortex. Roll vortices were thought to be associated with more than 50% of SBs. The SB frontal structure, in cross section parallel to the coast, is shown for the event of a SB passing Sydney Airport on December 11, 1972 (Fig. 7). Streamlines represent airflow relative to the circulation centres of the roll vortices and straight arrows indicate wind direction. The first circulation cell corresponds with the 28 minute period following the first wind change and the second cell with the subsequent two-hour period (Colquhoun et al., 1985). A possibly similar structure appears in the visible satellite imagery on October 6, 2015 (within the green circle of **Error! Reference source not found.**). The roll cloud in the lower atmosphere often exhibits a distinctive flow pattern. Winds near the surface in the horizontal propagating vortices exceed the speed of the propagation and can be a severe hazard to aircraft operating at low altitude (Christie, 1983).

Figure 7: Schematic representation deduced from wind temperature data, of the frontal structure in a vertical cross section parallel to the coast. Streamlines are airflow relative to the circulation centres of roll vortices and straight arrows are wind directions (Colquhoun et al., 1985).

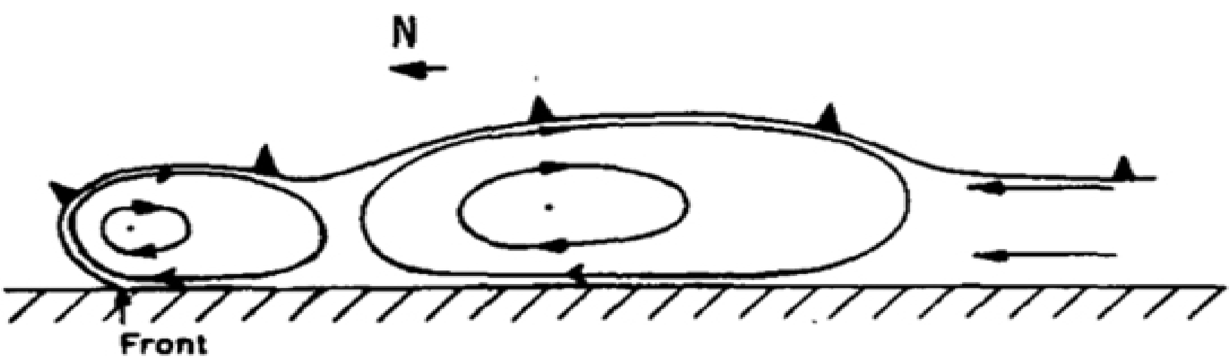

Figure 8: Schematic of the cloud signatures of a Southerly Buster that can be detected using several sources of satellite imagery. From https://sites.google.com/site/cmsforsh/CoE-Australia/shallow-cold-fronts/cloud-structure-in-satellite-images.

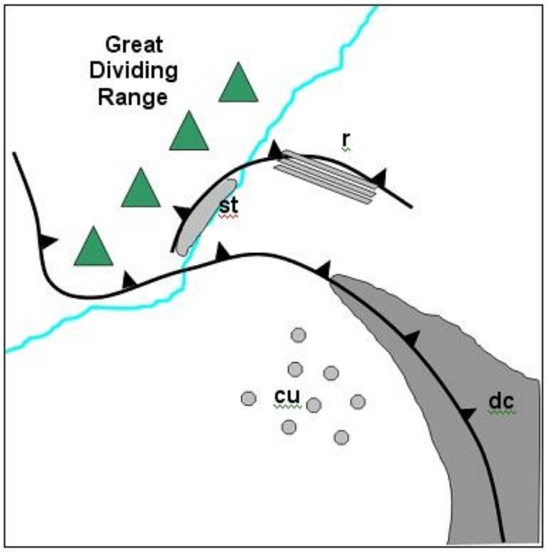

Figure 8 is a schematic of SB cloud signatures detected by the satellite imagery. The acronym, dc, indicates deeper cloud associated with the cold front (seen in visible, infrared, and water vapour images); st refers to low (stratus) cloud banking up against the escarpment of the range behind the SB (from visible and, sometimes, infrared images); r denotes roll clouds may be associated with the buster (from visible and, sometimes, infrared images). Finally, cu signifies open cell (speckled) cumulus cloud behind the cold front (from visible and infrared images)

As mentioned earlier in this section cloud features associated with the SB also were detected from the Himawari-8 visible imagery at 2140UTC on October 6, 2015 (Fig.6). The green arrow indicates the leading edge of the SB accompanied by a roll cloud. The roll cloud is consistent with the schematics of Figs. 7 and 8. The yellow arrow points to the low cloud banking up against the escarpment of the range behind the passage of the SB over eastern Great Dividing Ranges. The pink arrow provides the location of the parent cold front to the SB which is consistent with the schematic (Fig. 8). The red arrow (Fig.6) shows a wave train of solitary waves that propagated ahead of the roll cloud, as expected from Section 3.2, below. Both the solitary waves and the single roll cloud may sometimes be seen at the head of the SB in the visible imagery although this is not clear in the corresponding infrared images. They can produce wind shear which is sufficiently strong enough to pose a hazard to aircraft operating at low altitudes (typically landing or taking off). Solitary waves in the lower atmosphere take the form of rows of isolated, single-crested gravity, or gravity-inertia waves, which propagate predominantly as clear-air disturbances in a boundary layer inversion waveguide. (Christie, 1983).

Microwave scatterometer data, such as the winds from the advanced scatterometer (ASCAT) in Figure 9, also are useful for monitoring SBs, despite this polar orbiting satellite providing data of relatively limited temporal frequency. Fortunately, in this case, descending data was available at 2325UTC October 6 (Fig. 9). The wind change zone propagated to the north of 32S, and also was detected by the Himawari-8 visible imagery from 2020UTC to 2320UTC (Fig. 10). Using both red square boxes in Figs. 9 and 10, the SB was well represented for assessing the horizontal structures of the wind change, and for clouds. The transient wind horizontal wind shear in the red box of Figure 9 clearly is associated with the roll cloud in Figure 10. The wind speeds behind the change were about 10-15m/s, which were responsible for the stratus low clouds near the coast.

Figure 2: ASCAT winds at 2325UTC on October 6, 2015. Note the detailed near-surface winds, associated with the passage of the SB, in the red square. Image is from the NOAA/NESDIS website at https://manati.star.nesdis.noaa.gov/datasets/ASCATData.php

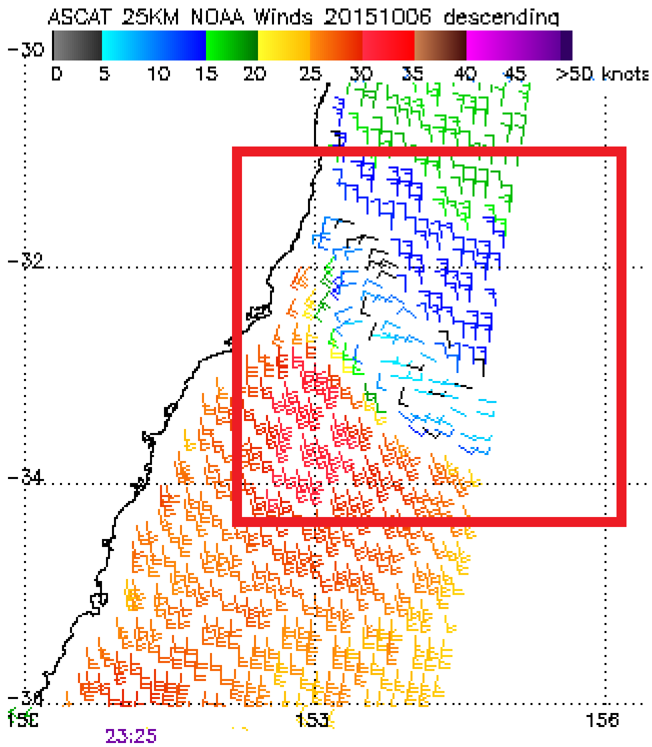

Figure 3: The Himawari-8 satellite visible images from 2020UTC to 2320UTC on October 6, 2015. a) 2020UTC, b) 2120UTC, c) 2220UTC, d) 2320UTC. The green arrow indicates the leading edge of the SB, which is accompanied by a roll cloud. The red arrow shows a train of solitary waves. The solid red line is the distance between the roll cloud and the wave train. The red square in d) is consistent with the red square area in

Figure 2.

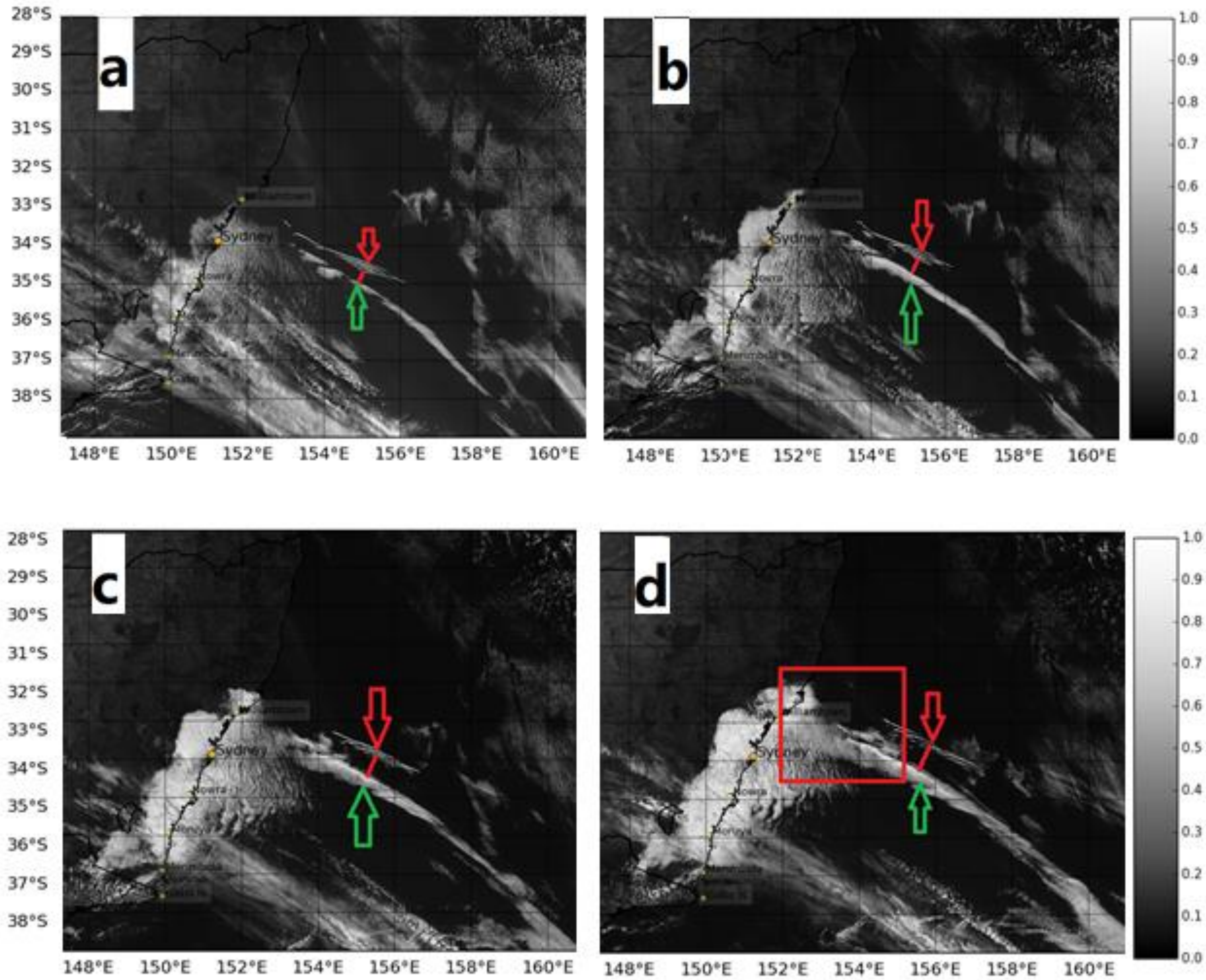

2.4 Radiosonde Data

Figure 4: Radiosonde profile on October 6, 2015, (permission from the Australian Bureau of Meteorology) a) at 1700UTC at Nowra Airport (YSNW), b) at 1900UTC at Sydney Airport (YSSY). Light brown left vertical axis is pressure (hPa); left black vertical axis is height above sea surface in hundreds of feet. So, e.g., 050 means 5000ft (about 1600m) above the sea surface. Right vertical axis is wind profiler information. The red solid lines are the temperature profile (right), and the dew point profile (left). Wind speeds are in m/s; short bar = 2.5 m/s, long bar = 5 m/s.

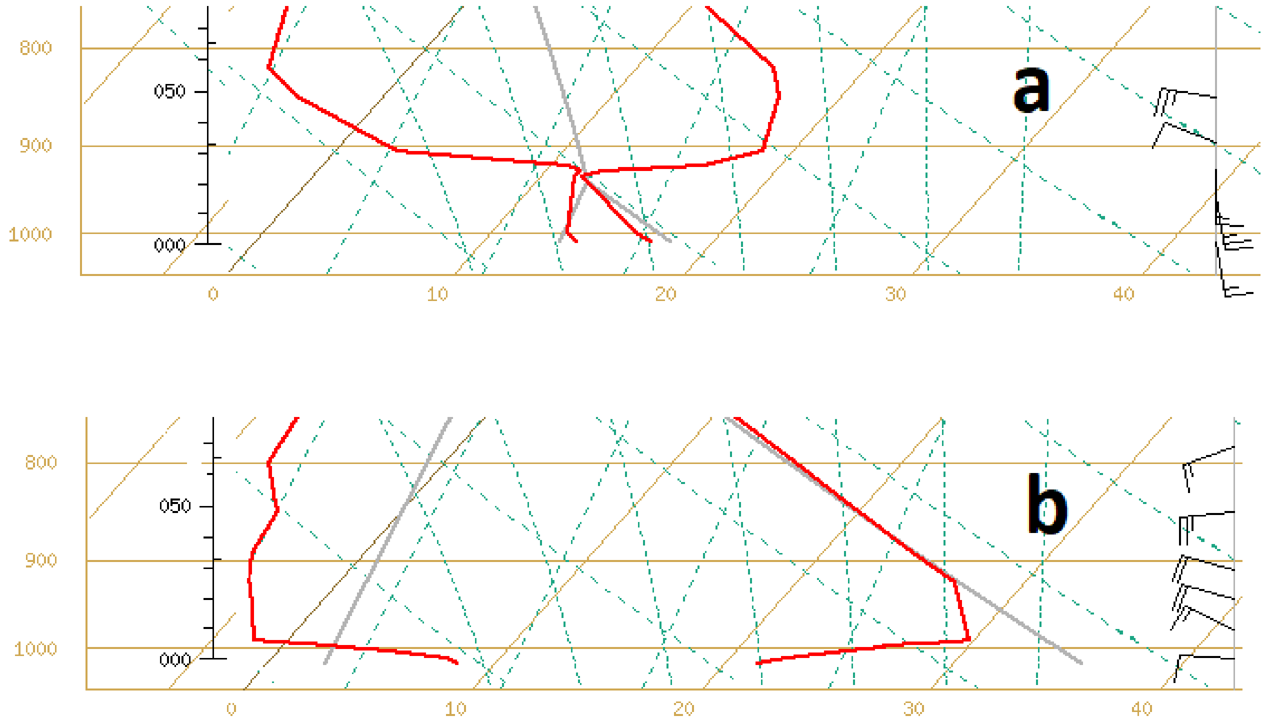

The vertical structure of the atmosphere can be inferred from sounding data from Nowra (YSNW) in Figure 4 (a), and Sydney (YSSY) in Figure 4 (b). Solitary waves observed in the lower atmosphere typically take the form of rows of isolated, single-crested waves which propagate predominantly as clear-air disturbances in a boundary layer inversion waveguide. The 1700 UTC sounding at YSNW (Figure 4 (a)), which commenced one hour after the SB passage, shows a low-level stable layer to 900hPa overlain by a well-mixed, nearly isentropic layer (neutral layer) extending up to 820hPa. This configuration is attributed to the advection of the deep continental mixed layer eastwards across the GDR, and then lying over a lower stable marine layer maintained by sea breeze activity along the coast (Holland and Leslie, 1986). The low-level southerly winds indicate that the cold air extended to about 800m (934hPa) above mean sea level (MSL). This shallow, stable boundary layer was capped by a strong inversion extending to 1000m (907hPa) above MSL. The corresponding temperatures were 11.8°C (at 934hPa) and 18.8°C (at 907hPa).

The dewpoints were 10.8°C and 14.2°C, respectively, significantly higher than those above the inversion (Table 1). The dewpoint depressions were no more than 5° below the inversion, then increased abruptly to 20°C at 850hPa. The winds were moderate to strong southerly below the inversion, and moderate to strong west to north-westerly above the inversion.

Table 1: The Nowra (YSNW) radiosonde data on 1700UTC October 6, 2015, after the SB passage. Nil means no data is available. Note the near-surface stable layer, topped by a neutral layer.

Pressure (hPa)	*Temperature (°C)*	*Dew point temperature (°C)*	*Wind Direction (degrees)*	*Wind Speed (knots) and m/s*
1023.6	17.5	14.2	170	19 (9.6m/s)
1011	17.4	14.1	170	17.4 (8.5m/s)
1000	16.4	13.4	170	22.6 (11.4m/s)
957	Nil	Nil	170	26.8 (13.7m/s)
934	11.8	11.5	nil	Nil
929	12.6	11.6	nil	Nil
926	Nil	Nil	180	14.4 (7.4m/s)
923	16.8	10.8	nil	Nil
907	18.8	2.8	nil	Nil
896	Nil	Nil	290	10.2 (5.2m/s)
850	17.4	-3.6	280	24.6 (12.5m/s)

At 1900UTC at Sydney, just ahead of the southerly change, the sounding revealed a strong, shallow inversion from the surface to 50m above MSL (1000hPa). Hence, the southerly change is very shallow with an overlying deep inversion. Fronts with a north-west/south-east orientation can experience blocking by the coastal mountain ranges (**Error! Reference source not found.**) of southeast Australia and progressively increase propagation speed on the eastern (coastal) side of the ranges while moving more slowly on the western side of the ranges. The effect is more pronounced for shallow cold fronts than those with the cold-air layer exceeding the height of the ranges (Coulman, 1985).

3. Density Current Theory: Application to SBs.

Most of the pressure changes in the postfrontal air of cold fronts are attributable to the density difference between the pre- and post-frontal air masses, and the rate at which the cold air deepens. Propagation speeds also are strongly affected by changes in the density difference (Colquhoun et al., 1985). It is noted that a more rigorous treatment of density currents in stratified shear flows is provided by Liu and Moncrieff (1996), but is beyond that needed in this study. The potential temperature cross-sections in Figure 7(b) of Colquhoun et al., (1985) are indicative of a density current. The dynamics of coastal ridging is well-described by the hydrostatic approximation, and the shallow-water equations of motion are applicable (Gill, 1977; Reason and Steyn, 1992). The vertical structure of the coastal atmosphere consists of an inversion, separating a roughly constant density cool marine lower layer from a deep upper layer with weak winds. Note that CTDs do not require the presence of an ocean to exist; it is the presence of stable stratification beneath the crests of the mountain barrier that is essential. There are well-known trapped disturbances occurring over interior plains and confined against large continental mountain ranges elsewhere around the world including, for example, the Rocky Mountains and the Himalayas (Reason, 1994)

3.1 Density Current Speed

The density of dry air is calculated from the ideal gas law, expressed as a function of temperature and pressure:

$$\boldsymbol{\rho = P/RT} \,, \qquad (1)$$

Where ρ =air density (kg/m³), P = absolute pressure (Pa), T = absolute temperature (K), and R = specific gas constant for dry air (287.058 J/(kg·K)).

In the atmosphere, density currents involve the flow (mass transport) of denser air moving into less dense air. For a single layer, the density current flow speed is:

$$\mathbf{c} = \sqrt{\boldsymbol{gH}}. \quad (2)$$

In a two-layer system, which is a good assumption for a SB, with cool air of density $\boldsymbol{\rho 1}$ moving into warm air of lower density $\boldsymbol{\rho 2}$, the density current flow speed is:

$$\boldsymbol{c_{DC}} = \sqrt{\boldsymbol{g'H}}\,, \quad (3)$$

Where the reduced gravity, $\boldsymbol{g'}$ (m/s^2) is:

$$\boldsymbol{g'} = \boldsymbol{g}\,(\boldsymbol{\rho 1} - \boldsymbol{\rho 2})/\boldsymbol{\rho 1} \quad (4)$$

In this case, the density current speed can be estimated, using radio sounding data from the YSNW station.

From Equation (1) and Table 1, for a cooler, denser lower layer overlain by a warmer, less dense upper layer:

$\boldsymbol{\rho_1} = \boldsymbol{P1/RT1}$ = 934/(287.058*284.8)= 0.0115,

$\boldsymbol{\rho_2} = \boldsymbol{P2/RT2}$ = 907/(287.058*291.8) = 0.0108.

Hence, $\mathbf{c} = \sqrt{\boldsymbol{g'H}}$, the density current speed

Where $\boldsymbol{g'} = \boldsymbol{g}(\boldsymbol{\rho_1} - \boldsymbol{\rho_2}) / \boldsymbol{\rho_1}$= 0.597, (5)

and, H, the cold air depth (m) at YSNW, is approximately 500m, from **Error! Reference source not found.**.

So, the density current speed, $\mathbf{c}_{\boldsymbol{DC}} = \sqrt{\boldsymbol{g'H}} = \sqrt{\mathbf{0.597 * 500}}$ = ~17m/s (~ 33knots). (6)

The estimated speed in (6) is consistent with the observational data from both the YSNW station observations and also the satellite wind data of

Figure 2 and 10, in which the winds in the red square behind the change are approximately 15m/s (~29knots). However, it is important to note that the calculation of $\mathbf{c}_{DC}$ is highly dependent on the value of ***H*,** so care was taken in selecting the value of H from detailed orographic maps.

3.2 The Solitary Waves Speed

It is likely that the parallel cloud lines in the red arrow area solitary waves (**Error! Reference source not found.**), ahead of the SB roll cloud. They are moving slightly faster than the roll cloud (DC). There are at least two possible explanations. One is that trapped density currents can produce solitary waves that are nonlinear Kelvin waves, which move faster than the density current speed (e.g., Ripa, 1982), so they propagate through and ahead of the leading edge of the density currents (Reason and Steyn, 1990; Reason et al., 1999). The presence of the solitary waves accounts for some of the difficulties in interpreting the precise nature of the leading edge of CTD over coastal southeast Australia. However, there was insufficient observational data before the Himawari-8 satellite, a high spatial and temporal resolution satellite, became available. The Himawari-8 data shows the solitary waves in the visible satellite imagery. A second possibility is that the solitary waves are inertia-gravity waves, also known as Poincaré waves. Like non-linear Kelvin waves, Poincaré waves also travel faster than the density current. It was decided to proceed with the assumption that the solitary waves are inertia-gravity waves, because non-linear Kelvin waves eventually break. However, there is no clear sign that the observed solitary waves in this study do break; instead they appear to dissipate after they move well away from the cold front. The formula for the calculation of the phase speed of inertia-gravity (Poincaré) waves is very well-known (e.g., Gill, 1982), and is given by:

$$\boldsymbol{c_{poincar\acute{e}}} = \sqrt{\boldsymbol{g'H}}\left(\mathbf{1} + \frac{\boldsymbol{f_0^2}}{\boldsymbol{g'\ Hk^2}}\right)^{\mathbf{1/2}} = \mathbf{c}_{\boldsymbol{DC}}\left(\mathbf{1} + \frac{\boldsymbol{f_0^2}}{\boldsymbol{g'\ Hk^2}}\right)^{\mathbf{1/2}} \tag{7}$$

Where:

$c_{poincaré}$ = Poincaré wave phase speed (m/s), and

c_{DC} = Density current speed (m/s)

g' = Reduced gravity(m/s^2)

f_0 =Coriolis parameter （$f = 2\Omega \sin \varphi$),

Where the rotation rate of the Earth, Ω = 7.2921×10^{-5}rad/s, can be calculated as 2π/T radians per second, φ = latitude (Nowra is 34.93°S), and H = the cold air depth (m), at Nowra (500m)

The Rossby radius of deformation, **L** = $\frac{\sqrt{g'\ H)}}{f} = \frac{\sqrt{0.597*500}}{8.35\times 10^{-5}}$ = 204km, where

$$f_0 = 2\Omega \sin\varphi = 2 * 7.2921 \times 10^{-5} * \sin(34.93) = 8.35 \times 10^{-5}$$

$$g' = (g(\rho_{lower} - \rho_{upper})) / \rho_{lower} = 0.597$$

Rossby radius of deformation L = $\frac{\sqrt{g'\ H)}}{f_0} = \frac{\sqrt{0.597*500}}{8.35\times 10^{-5}}$ = 204km

Wave number k =2π/wavelength, where wavelength is the Rossby radius of deformation. Thus:

$$\mathbf{k^2} = (\frac{2\pi}{L})^2 = (\frac{2\pi}{2.04 * 10^5})^2$$

Hence, $c_{poincaré} = c_{DC}(1 + \frac{f_0^2}{g'\ Hk^2})^{1/2} = 1.197 * c_{DC} = \sim 1.2 * c_{DC}$ (8)

From Eq. 8, the inertia-gravity waves move about 20% faster than the density current. This difference can explain how, in **Error! Reference source not found.** and 10, the waves move increasingly ahead of the main southerly change, because they are propagating faster than the southerly change.

Table 2: Details of the low level structure of the inversion at Nowra (YSNW).

Pressure (hPa)	*Temperature (°C)*	*Absolute temperature (°K)*
934	11.8	284.8
907	18.8	291.8

4. Discussion and Conclusions

This study was intended primarily to be a detailed analysis of the southern buster (SB) event of October 6-7, 2015. The parallel cloud lines, revealed by the high resolution imagery, appear to be solitary waves, and are travelling ahead of the SB along the New South Wales coast. This study has a major advantage over earlier SB studies, due to the access to the much higher temporal and spatial resolution of the Himawari-8 satellite imagery, and other data. The study supported the concept of a SB as a coastal trapped density current, from both the observations, and also from the accuracy of the results obtained from the simple density current model. A simple density current model was used to estimate the propagation speed of the SB density current. The estimate of 17m/s for the density current speed was close to the observed wind speed of about 15m/s at Nowra airport. The calculated phase speed of the solitary waves, when assumed to be inertia-gravity (Poincaré) waves was about 20% greater than the speed of the density current. Again, this difference was consistent with the satellite imagery, which showed the solitary waves increasingly moving away from the leading edge of the SB. Observations at YSNW and YSSY both exhibit the common characteristics of a classical SB, with an abrupt change in winds, temperatures and pressure. The corresponding synoptic weather charts illustrate that, during the SB event a high pressure ridge, also referred to as a coastally trapped disturbance, and generated the SB along the south eastern Australian coast. Meanwhile, the main high-pressure cell had moved only a few hundred kilometres to the east.

Some interesting questions were raised during the study, and will be addressed in future work. Questions raised include the following, and some speculation is made concerning possible answers to these questions. Moreover, answers will be sought from a planned series of very high resolution numerical modelling simulations of the October 6-7, 2015 SB event.

One key question is to determine why was the SB stronger and longer-lasting at Sydney airport than at Nowra airport? Possible reasons include the influence of the differences in orography, differential continental heating and differential friction between land and sea. Each of these possible explanations was suggested by (Garratt, 1986), but supporting observational and modelling evidence was not available at that time. Also, there is related speculation on the effects of coastal irregularities, changes in coastal alignment, and land-sea temperature gradients (Holland and Leslie, 1986); some of these influences possibly affect the speed and duration of the SB. One factor is the greater distance of Nowra airport from the coast, about 20km; whereas the runways of Sydney Airport are adjacent to the water. The Nowra airport location will experience larger frictional effects from the land, which could decouple the motion towards to the north and reduce the propagation speed. Another factor is the possible effects of station elevation: the elevation of Nowra Airport is 109m, while Sydney Airport is only about 6m. As stated above, the southerly change is shallow cold air travelling along the coast under the warmer air. From Section 3, the speed of the SB depends on the depth of the cold air according to the formula $c = (g'H)^{1/2}$, where g' is the reduced gravity, and H is the depth of the SB. So, as the cold air depth at Nowra Airport is less than at Sydney Airport, the wind speeds in Nowra Airport can be expected to be weaker than at Sydney Airport. An additional possibility is due to the impact of the Illawarra escarpment, west of the Illawarra coastal plain, south of Sydney, with escarpment heights ranging from 300 to 803 meters. When the southerly winds travel from Nowra, past Kiama and Wollongong to Sydney, they are blocked from spreading westwards, so cold air mass accumulates along the escarpment and its depth must increase. When they move away from the escarpment, the deeper cold air trapped against the escarpment is released, thereby progressively increasing its propagation speed towards the Sydney Basin, producing stronger southerly winds. A very recent example of the influence on a SB of the Illawarra escarpment and of the station height above sea level, is that of 31 January 2019, as shown in Table 4.

Table 4: Southerly Buster of 31 January 2019 illustrating differences in maximum gust speed and times at locations Bellambi and Wattamolla adjacent to the Illawarra escarpment and YSNW in the south to Kurnell/YSSY in the Sydney basin to the north.

AWS station	*Max. wind gust (km h^{-1}) & direction*	*Time (Local)*	*Station height above sea level (m)*
YSSY	S 91 (25.3 ms^{-1})	18:17	6
Kurnell	S 87 (24.2 ms^{-1})	17:07	4
Wattamolla	SSE 107 (29.7 ms^{-1})	16:16	44
Bellambi	SSW 85 (23.6 ms^{-1})	16:20	10
YSNW	S 81 (22.5 ms^{-1})	14:30	109

Table 4 indicates how the maximum wind gusts increase from 22.5 m/s at Nowra airport to 23.6 m/s Belambi and 29.7 m/s at Wattamolla, then decrease to 24.2 m/s at Kurnell and 25.3 m/s at Sydney airport, after entering wider Sydney basin. Note also the differences in height above sea level of Nowra airport and Wattamolla compared to the other stations. Other interesting questions include why the maximum gust at Sydney airport was about 50 minutes after the maximum gust at Kurnell, when the distance between those two locations is only about 10 km; and was the height difference above sea level between Bellambi and Wattamolla the reason the maximum gust occurred at Wattamolla before Bellambi. As mentioned above, a series of planned high resolution numerical modelling studies hopefully will provide further insight into the questions raised.

Finally, it is noteworthy that the solitary waves extend east as far as 157^0 E on the Himawari-8 satellite visible image (Fig. 10), which raises the question of how far east they can travel, and has possible safety implications for landing/take-off at Lord Howe Island airport. Again, this question can best be answered with a combination of observations and high-resolution numerical modelling.

Acknowledgments

The authors wish to acknowledge the Australian Bureau of Meteorology for providing the data used in this study. The study also was partially funded by the School of Mathematical and Physical Sciences at the University of Technology Sydney.

References

Baines, P. G., 1980: The dynamics of the southerly buster. *Australian Meteorological. Magazine*, 28, 175–200.

Christie, D.R. 1983. Solitary waves as aviation hazards, *Eos Trans*. AGU, 64, 67.

Clarke, R.H. 1961. Mesostructure of dry cold fronts over featureless terrain. *Journal of Meteorology*., 18, 715-735.

Colquhoun, J.R., Shepherd, D.J., Coulman, C.E., Smith, R.K. and McInnes, K. 1985. The Southerly Burster of south eastern Australia: An orographically forced cold front. *Monthly Weather Review*., 113, 2090-2107.

Coulman, C. 1985. Orographically forced cold fronts: mean structure and motion, *Boundary-Layer Meteorology*., Dordrecht, Holland, 57-83.

Egger, J., and K. P. Hoinka, 1992. Fronts and orography. *Meteorology and Atmosheric Physics*, 48**,** 3–36.

Garratt, J. 1986. Boundary-layer effects on cold fronts at a coastline. *Boundary-Layer Meteorology*., 101-105.

Gentilli, J. 1969. Some regional aspects of southerly buster phenomena. *Weather*., 24, 173-184.

Gill, A.E. 1977. Coastally trapped waves in the atmosphere, *Quarterly Journal of the Royal Meteorological Society*., 431-440.

Gill, A.E. 1982. Atmosphere-Ocean Dynamics. Academic Press. London. Chapter 8.

Holland, G.J. and Leslie, L.M. 1986. Ducted coastal ridging over S.E. Australia, *Quarterly Journal of the Royal Meteorological Society*., 731-748.

Shallow Cold Fronts. In: http://www.eumetrain.org (Editor). The full website address is http://www.eumetrain.org/satmanu/CMs/ShCF/navmenu.php?page=2.0.0.

Liu, C.-H., and M. W. Moncrieff, 1996: A numerical study of the effects of ambient flow and shear on density currents. *Monthly Weather Rev*iew.,124, 2282–2303.

Mass, C. E., and M. D. Albright, 1987: Coastal southerlies and alongshore surges of the west coast of North America: Evidence of mesoscale topographically trapped response to synoptic forcing. *Monthly Weather Review*.,115, 1707–1738.

McInnes, K. L., 1993b: Australian southerly busters. Part III: The physical mechanism and synoptic conditions contributing to development. *Monthly Weather Review*.,121, 3261–3281.

Reason, C., 1994. Orographically trapped disturbances in the lower atmosphere: Scale analysis and simple models, *Meteorology and Atmosheric Physics*., 53, 131-136.

Reason, C.J.C. and Steyn, D.G., 1990. Coastally trapped disturbances in the lower atmosphere: dynamic commonalities and geographic diversity. *Progress in Physical Geography*., 14, 178-198.

Reason, C.J.C. and Steyn, D.G. 1992. Dynamics of Coastally Trapped Mesoscale Ridges in the Lower Atmosphere. *Journal of Atmospheric Science*., 49, 1677-1692.

Reason, C.J.C., Tory, K.J. and Jackson, P.L. 1999. Evolution of a Southeast Australian Coastally

Trapped Disturbance. *Meteorology and Atmospheric Physics*., 70, 141-165

Reid, H. and Leslie, L.M. 1999. Modeling coastally trapped wind surges over southeastern Australia. Part I: Timing and speed of propagation. *Weather and Forecasting*., 14, 53-66.

Ripa, P. 1982. Nonlinear wave-wave interactions in a one-layer reduced-gravity model on the equatorial beta-plane. *Journal of Physical Oceanography*., 12, 97–111.